Ecotoxicology and Environmental Safety 158 (2018) 230–238

Contents lists available at ScienceDirect

Ecotoxicology and Environmental Safety

journal homepage: www.elsevier.com/locate/ecoenv

Assessing the influence of humic acids on the weathering of galena and its environmental implications

Qingyou Liu[a], Heping Li[a,*], Guoheng Jin[a,b], Kai Zheng[a,b], Luying Wang[a,b]

[a] Key Laboratory of High-Temperature and High-Pressure Study of the Earth's Interior, Institute of Geochemistry, Chinese Academy of Sciences, Guiyang 550081, China
[b] University of Chinese Academy of Sciences, Beijing 100039, China

ARTICLE INFO

Keywords:
Humic substances
Galena
Anglesite
Electrochemical method
Fourier transform infrared
Raman

ABSTRACT

Galena weathering often occurs in nature and releases metal ions during the process. Humic acid (HA), a critical particle of natural organic matter, binds metal ions, thus affecting metal transfer and transformation. In this work, an electrochemical method combined with spectroscopic techniques was adopted to investigate the interfacial processes involved in galena weathering under acidic and alkaline conditions, as well as in the presence of HA. The results show that the initial step of galena weathering involved the transformation Pb^{2+} and S°, regardless of whether the solution was acidic or alkaline. Under acidic conditions, S° and Pb^{2+} further transform into anglesite, and HA adsorbs on the galena surface, inhibiting the transformation of sulfur. HA and Pb (II) ions form bridging complexes. Under alkaline conditions without HA, the sulfur produced undergoes no transformation, whereas Pb^{2+} will transform into PbO. The presence of HA changes the galena weathering mechanism via ionization effect, and Pb^{2+} is ultimately converted into anglesite. Higher acidity in acidic conditions or higher alkalinity in alkaline conditions causes galena corrosion when the electrolyte does not contain HA. Conversely, higher pH always accelerates galena corrosion when the electrolyte contains HA, whether the electrolyte is acidic or alkaline. At the same acidity/alkalinity, increasing the concentration of HA inhibits galena weathering. Galena will release 134.7 $g\,m^{-2}{\cdot}y^{-1}$ Pb^{2+} to solution at pH 2.5, and the amount decreases to 28.09 $g\,m^{-2}{\cdot}y^{-1}$ in the presence of 1000 mg/L HA. This study provides an in situ electrochemical method for the assessment of galena weathering.

1. Introduction

Galena, one of the most common lead-bearing sulfide minerals, can easily weather when exposed to oxidizing conditions and form more stable secondary lead species (Benvenuti et al., 2000; Keim and Markl, 2015). In natural geologic environments, anglesite and cerussite are most often transformed during galena weathering (Lara et al., 2011; Szczerba and Sawlowicz, 2009). During the galena weathering process, heavy metals, such as Pb, As, and Cr, are released and cause ecological risk to the soil-plant system and the sediment-water column (Azhari et al., 2017). In a laboratory setting, Hsieh and Huang (1989) were the first to systematically study the dissolution of PbS(s) in dilute aqueous solutions. The results show that the dissolution reaction is pH dependent, enhanced by dissolved oxygen and slightly affected by photo-irradiation. The overall dissolution processes is controlled by surface reaction. Based on this study, Fornasiero et al. (1994) used Fourier transform infrared spectroscopy and X-ray photoelectron spectroscopy to investigate the surface oxidation of galena subject to various conditioning environments. They proposed a mechanism of oxidation involving the dissolution of lead and sulfide ions, the formation of lead sulfoxy species and lead carbonate, and their subsequent adsorption or precipitation on the galena surface. Similarly, they determined the oxidation reaction is pH dependent, and the oxidative dissolution of PbS(s) occurs primarily by the reaction (1), as Hsieh and Huang (1989) reported. In recent years, isotope technique has been a useful tool for the investigation of galena oxidation. Heidel and Tichomirowa (2011) investigated galena oxidation mechanisms via oxygen and sulfur isotopes. The oxygen isotope composition of sulphate produced from galena oxidation could be determined for the first time. Sulfur isotopes of sulphate showed an enrichment of (32) S° in sulphate (relative to galena), which increases with increasing pH. Moreover, its enrichment processes may be associated with the formation of anglesite.

$$PbS \rightarrow Pb^{2+} + S^{\circ} + 2e^{-} \quad (1)$$

Under natural conditions, many studies (Acero et al., 2007; Gerson and O'Dea, 2003; Keim and Markl, 2015; Mikhlin et al., 2006; Ryan et al., 2001) have revealed the mechanism of galena weathering via

* Corresponding author.
E-mail address: liheping123@yahoo.com (H. Li).

https://doi.org/10.1016/j.ecoenv.2018.04.030
Received 30 January 2018; Received in revised form 14 April 2018; Accepted 17 April 2018
Available online 27 April 2018
0147-6513/

electrochemical methods and surface observation. The products include (1) the formation of chloropyromorphite by the addition of phosphate to Pb-contaminated soil, which has been proposed as a remediation technology to reduce the mobility and bioavailability of Pb; (2) acidic aerobic dissolution to form H_2SO_4 and $Pb^{2+}{\cdot}6H_2O$ (Gerson and O'Dea, 2003); (3) the formation of acceptor-type cation vacancies $Pb_{1-x}S$ (Mikhlin et al., 2006); and (4) the formation of a lead-deficient and sulfur-rich surface layer, which is consistent with the observed non-stoichiometry between dissolved sulfur and lead in acidic environments. Acero et al. (2007) revealed that galena dissolution is controlled by diffusion processes or by the mixed-controlled diffusion of reactants and products between the bulk solutions and the reacting surfaces. Based on the above research, Keim and Markl (2015) explained the weathering of galena in detail, and they presented hydro-geochemical models of Pb dissolution and re-precipitation during the weathering of ore deposits containing galena. Generally, galena weathering is an electrochemical process. Different lead or sulfur intermediate products may occur, but the consensus is galena oxidative dissolution occurs first via reactions (1) (Paul et al., 1978). Then, Pb^{2+} or S° further transform, depending on the conditions.

HA is known to comprise supra-molecular structures of small biomolecular fragments bound together through cation bridging, hydrogen bonding and hydrophobic interactions (Sutton and Sposito, 2005). HA has two polar functional groups, a phenolic group and a carboxylic group, and the dissociated groups can easily bind to metal ions (Ondrasek et al., 2018). Thus, these groups might control metal transfer and transformation (Liu and Gonzalez, 2000) and affect the mobility, toxicity and bioavailability of metal ions in the environment (Koopal et al., 2005; Schulten and Schnitzer, 1997). It is important to understand the nature of organic functional groups of HA in the process of determining the stability of metal complexes and the effects on environmental detoxification (Pandey et al., 2000). HAs may enhance or diminish heavy metal adsorption, depending on the relative stabilities of metal-humate binary and metal-humate-surface ternary complexes as a function of pH (Apak, 2002). It is known that HA forms negatively charged complexes with heavy metal ions (Yang and Van Den Berg, 2009). In accordance with hard and soft acid/base theory, Cu(II) and Pb (II) ions react with HA via O and N atoms and form stable complexes (Hizal and Apak, 2006). Most heavy metals are known to share common binding sites in humic substances (Tipping et al., 2002). Heavy metals and HA may form different complexes. For example, Pb^{2+} and HA can form bridging (Fig. 1a) or unidentate (Fig. 1b) HA-Pb(II) complexes (Jerzykiewicz, 2004).

For these reasons, the study of HA has attracted the attention of scientists in various fields (Genc-Fuhrman et al., 2016; Huang et al., 2017; Martin et al., 2017). In the geochemical processing of Au, Chotpantarat et al. (2015) revealed that HA can dissolve and transport Au because Au and HA can form a complex. Bergeron and Harrison (1989) confirmed the significance of humic substances in the chemical transport of Au and revealed an increase in Au solubility according to the following order: humic acid < fulvic acid < potassium humate. In the environmental field, acid mine drainage and heavy metal ion pollution from sulfide mineral oxidation are serious issues; the passivation of sulfide minerals prior to oxidation has been an efficient means to prevent these issues (Sahoo et al., 2013). HA is interesting because it has a relatively environmentally friendly way to block electrochemical activity through passivation of the electrode surface (Acai et al., 2009), and it participates in high-affinity interactions with oxide surfaces (Li et al., 2015). It should be noted that HA itself is potentially toxic to humans, due to its acidity when partly dissolved in water, and thus, HA is not a suitable adsorbent without pre-treatment. The use of different physical-chemical methods to modify HA is one of the most common pre-treatment measures (Celebi and Erten, 2010; Jiang et al., 2014; Lei et al., 2016).

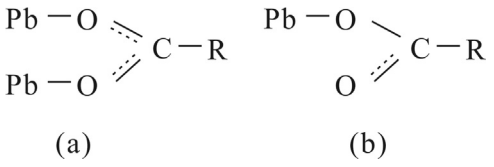

Fig. 1. Modes of coordination of Pb (II) ions to carboxyl groups in HA. (a) bridging complexes, (b) unidentate complexes.

As mentioned above, galena is often weathered under natural conditions and releases metal ions during this process. Meanwhile, HA binds metal ions and, thus, affects metal transfer and transformation. Therefore, HA must affect galena weathering when both are exposed to the same near-surface oxidizing conditions, and these conditions are often present in Pb-Zn ore mines. To our knowledge, no data have been reported on the effects of HA during galena weathering. In this work, polarization spectroscopy and electrochemical impedance spectroscopy (EIS) were used to investigate galena weathering under different concentrations of HA with different pH values, with aimed to (1) reveal the galena electrochemical behaviors in the presences of HA and (2) quantitatively determine how HA concentration and pH affect galena weathering.

2. Materials and methods

2.1. Galena electrode

Galena samples were collected from the Huize Pb-Zn deposit (Yunnan Province, China). X-ray powder diffraction analysis showed that the samples were composed of PbS and ZnS, and the electron microprobe tests revealed the percentages of the elements Pb, Zn and S (wt%) were 86.53%, 0.0064% and 13.39%, respectively. The galena samples were cut into an approximately cubic shape to guarantee their bottom surface, namely the working area, was 0.25 cm^2. Then, the samples were connected to a copper wire using silver paint on the upper surface and sealed with epoxy resin, keeping only the working surface exposed to the solution (Liu et al., 2017; Wang et al., 2016). Muñoz et al. (1998) reported this detailed electrode preparation method. Prior to each test, the mineral electrode was polished with 1200-grit carbide paper to obtain a fresh surface, degreased using alcohol, rinsed with deionized water and dried in a stream of air.

2.2. HA electrolyte

HA (CAS 1415-93-6, Shanghai Aladdin Bio-Chem Technology Co., LTD), with more than 90% (wt%) as fulvic acid (FA, $C_9H_9NO_6$), was used as the electrolyte. First, HA was dissolved in water to obtain 0, 10, 100 and 1000 mg/L electrolyte solutions. Then, HNO_3 and NaOH solutions were used to adjust the pH of the electrolyte solutions to 2.5, 4.5, 8.5 and 10.5, respectively.

2.3. Electrochemical measurements

As stated previously, galena weathering is an electrochemical process. Therefore, its weathering character and parameters were evaluated through electrochemical test. Electrochemical measurements were performed using a computer-controlled electrochemical measurement system (PARSTAT 2273, Princeton Applied Research) with a conventional three-electrode electrolytic cell that included a platinum auxiliary electrode, a pyrite working electrode and a saturated calomel reference electrode (SCE). All other potentials in this study are quoted with respect to the SCE (0.242 V vs. standard hydrogen electrode), if not otherwise stated. To minimize the resistance of the solution between the working electrode and the reference electrode, the reference electrode was connected to a Luggin capillary.

In this work, polarization curve and electrochemical impedance spectroscopy (EIS) were used to investigate the electrochemical

characteristics of galena weathering. Polarization curves allowed for immediate weathering rate information. EIS measurements were carried out at different AC frequencies, and analysis of the system response revealed information about the interface, its structure and reactions taking place there. The polarization curves were obtained by changing the electrode potential automatically from − 250 to + 250 mV (vs. open current potential, OCP) at a scan rate of 10 mV s^{-1}. The EIS tests were performed using the OCP in the frequency range of 0.001–10,000 Hz, with a peak-to-peak amplitude of 10 mV. ZSimpWin 3.20 (2004) software was used to fit the impedance data. To ensure reproducibility, identical experiments were repeated at least three times (the random errors of the results of all three identical experimental were within tolerance), and all results reported in this paper were averaged. The experiments were conducted at 25 ± 1 °C.

Prior to the polarization and EIS tests, OCP tests were performed. During the OCP experiments, the electrode potential increased for 5 min and reached a quasi-steady state, where the steady-state is defined here as a change of less than 2 mV per 5 min. Then, the electrode was stabilized for 400 s, and the potential was recorded as the OC potential. When the duplicate/triplicate experiments were performed, if the potential was not within ± 5 mV of the first experiment when the quasi-steady state was reached, the OCP test ceased. Then, a new replicate was performed to obtain the same OC potential as the first test when stabilized for approximately 400 s. In this work, the standard deviations of the experimental results no more than 3% were reported.

2.4. Surface characterization measurements

The surface morphologies of corroded samples were investigated by Fourier transform infrared (FTIR) spectroscopy and Raman spectroscopy. Seven 0.5 cm × 0.5 cm × 0.01 cm galena samples were used for FTIR analysis. The seven galena samples were immersed in seven different solutions: pH 4.5 without HA; pH 4.5 with 10 and 100 mg/L HA, respectively; pH 8.5 without HA; pH 8.5 with 10 and 100 mg/L HA, respectively, and the seventh solution was pH 8.5 with 100 mg/L HA plus 1 mg/L Pb^{2+}. All the samples were weathered for 10 weeks and then characterized using FTIR. FTIR spectra were collected on a Bruker Vertex 70 Fourier transform infrared spectrometer with an Attenuated Total Reflectance (ATR) accessory. The scanning range was 600–4000 cm^{-1} with a resolution of 4 cm^{-1} and 16 scans.

Four 1.0 cm × 1.0 cm × 0.2 cm galena samples were used for surface analysis. The four galena samples were immersed in four different solutions: (1) pH 4.5 with 100 mg/L HA, (2) pH 4.5 without HA, (3) pH 8.5 with 100 mg/L HA and (4) pH 8.5 without HA. The four pristine samples and the samples weathered for 10 weeks were characterized using Raman spectroscopy (British Renishaw inVia Reflex type microscopic confocal laser Raman spectrometer) at a wavelength of 514 nm and a collection time of 10 s. The laser power was 50 mW to avoid the destruction of the galena samples.

3. Results and discussion

3.1. Polarization curves study

Fig. 2 shows the potentiodynamic curves of the galena electrode at different concentrations of HA solutions. The potentiodynamic curves show that the galena electrode had a similar potentiodynamic profile, suggesting the same electrochemical interaction mechanism, in the

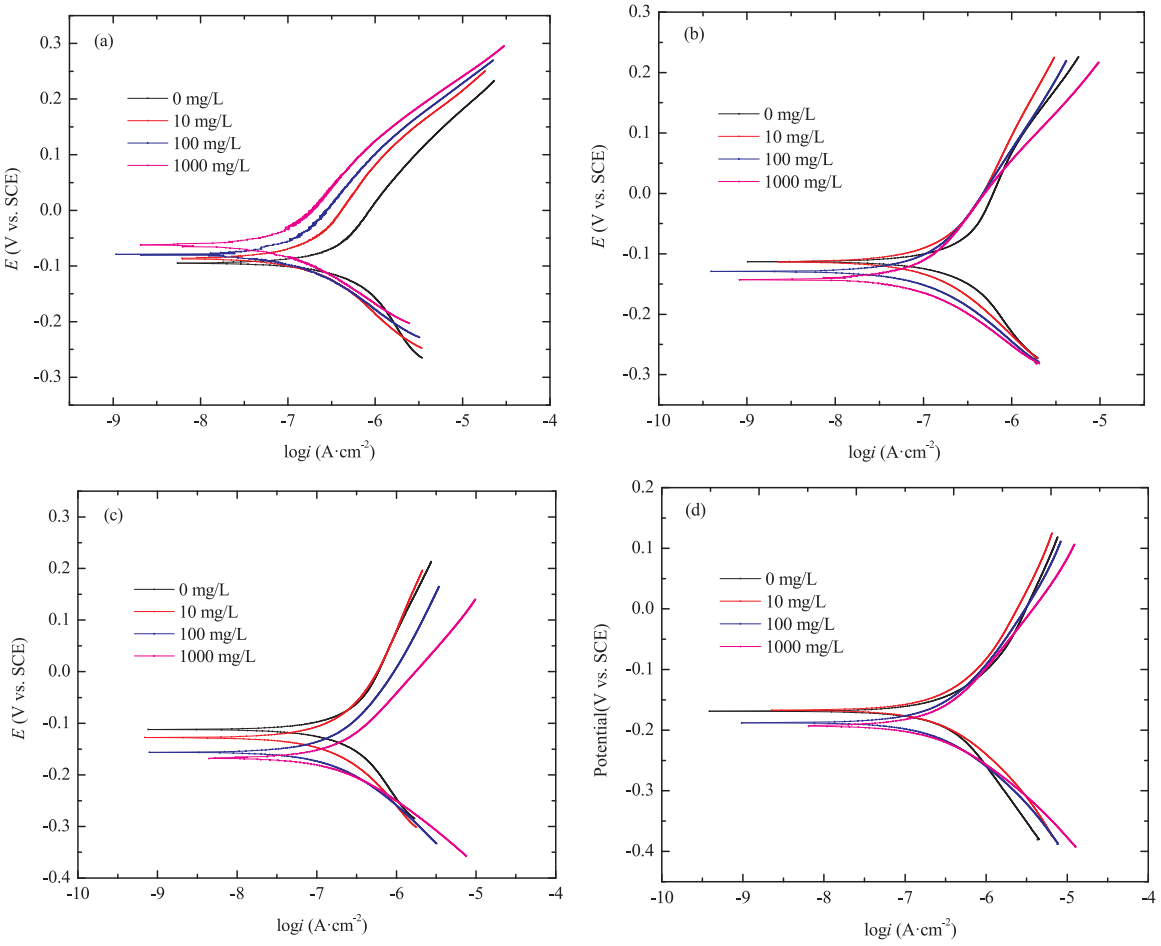

Fig. 2. Potentiodynamic curves of galena in different concentrations of HA solutions (25 °C, a: pH 2.5; b: pH 4.5; c: pH 8.5; d: pH 10.5).

Table 1
Electrochemical parameters of the galena electrode under different concentrations and acidities of HA solutions.

pH	C_{HA} (mg L^{-1})	E_{corr} (mV)	i_{corr} (μA cm^{-2})	b_c (mV)	b_a (mV)	R_p (KΩ cm^2)
2.5	0	− 93.20	0.398	168.83	213.62	103.0
	10	− 84.72	0.155	143.42	206.92	237.6
	100	− 75.46	0.105	100.32	192.57	273.1
	1000	− 59.34	0.083	97.46	169.90	324.4
4.5	0	− 112.51	0.303	192.84	294.63	167.2
	10	− 115.40	0.216	172.46	272.59	212.6
	100	− 128.89	0.143	132.84	236.42	258.6
	1000	− 140.18	0.107	102.16	177.36	263.4
8.5	0	− 115.79	0.469	300.48	457.58	168.1
	10	− 127.86	0.318	234.77	397.59	201.8
	100	− 156.05	0.246	198.14	372.05	228.5
	1000	− 163.20	0.137	134.60	202.91	256.8
10.5	0	− 162.60	0.815	325.66	282.64	80.7
	10	− 167.37	0.540	186.23	258.74	87.2
	100	− 187.64	0.382	168.30	213.37	107.1
	10.5	− 181.12	0.243	120.22	173.32	127.0

E_{corr}: corrosion potential; i_{corr}: corrosion current density; b_a: anode Tafel slope; b_c: cathode Tafel slope; R_p: polarization resistance.

presence or absence of HA electrolyte.

The galena polarization parameters, corrosion potential (E_{corr}) and corrosion current density (i_{corr}) were dependent on Tafel extrapolation (Bard and Faulkner, 2001), and polarization resistance R_p was also obtained from the Stern-Geary equation (Eq. 2) (Stern and Geary, 1957).

$$R_p = b_a b_c/[2.\ 3i_{corr}(b_a + b_c)] \quad (2)$$

For these electrochemical parameters, the parameter i_{corr} reflects the corrosion rate of the material. Specifically, the higher the density of current is, the faster the corrosion rate will be, while E_{corr} is related to the susceptibility of the material to corrosion. A negative value of E_{corr} means the material is difficult to corrode. A bigger Tafel slope indicates greater interaction resistance, i.e., unfavorable conditions for electrode interaction. The parameter R_p reflects the interaction resistance. A bigger R_p value means the electrode process changes more difficult. The detailed polarization results are listed in Table 1. The polarization results of galena samples exposed to different concentrations of HA revealed that at the same pH, a higher HA concentration resulted in a smaller corrosion density (i_{corr}). This suggests that HA inhibits the electrochemical corrosion of galena, which comes from the increasing resistance of the polarization of the galena samples.

When the pH of the HA electrolyte solution was 2.5 and the concentration of HA increased from 0 mg/L to 10 mg/L, the galena corrosion density (i_{corr}) decreased from 0.398 to 0.155 μA cm^{-2}. Then, the corrosion density decreased to 0.105 μA cm^{-2} at a HA concentration of 100 mg/L, and finally decreased to 0.083 μA cm^{-2} at a HA concentration of 1000 mg/L. Therefore, increasing the concentration of HA inhibits galena weathering, and the inhibiting efficiencies (η) were 61.06%, 73.62% and 79.15%, respectively. In material science, η is defined by Eq. (3) (Solmaz et al., 2008):

$$\eta = (i_{corr} - i^0_{corr})/i^0_{corr} \quad (3)$$

where i^0_{corr} and i_{corr} are the corrosion current densities without and with HA, respectively. The reaction involved in the natural weathering of galena is undoubtedly an electrochemical process, and the anodic reaction is expressed as reaction (1) (Paul et al., 1978). O_2 is reduced on the cathode (reaction (4)) when the electrolyte is acidic.

$$O_2 + 4H^+ + 4e^- \rightarrow 2H_2O \quad (4)$$

As mentioned previously, HA has two polar functional groups, a phenolic group and a carboxylic group. HA can ionize and release H^+ and $–COO^-$ ions. A higher concentration of HA releases higher concentrations of H^+ and $–COO^-$ ions. At the cathode, the higher concentration of H^+ is favorable for O_2 reduction, and this is the reason why the cathodic Tafel slope (b_c) decreased. At the anode, the higher concentrations of –COO- ions favor the oxidation reaction of the complexation of $–COO^-$ and Pb^{2+}. This complexation causes the anodic Tafel slope (b_a) to decrease. It seems that the higher concentration of HA promotes galena electrochemical corrosion, but other facts cannot be ignored. When the complexation of $–COO^-$ and Pb^{2+} is enhanced, more S° is also produced. Thus, when HA is present in higher concentrations, more HA and S° are absorbed on the electrode surface and passivate the galena electrode. This passivation results in an increase in the galena electrode polarization resistance (R_p), which causes the galena corrosion current density to decrease, and the galena weathering is weakened. When the pH of the HA electrolyte was 4.5, i_{corr} decreased from 0.303 to 0.216 μA cm^{-2} and to 0.143 μA cm^{-2} with increasing HA concentration from 0 mg/L to 10 mg/L and to 100 mg/L, respectively. Finally, the corrosion density reached 0.107 μA cm^{-2} when HA increased to 1000 mg/L. The inhibiting efficiencies were 28.71%, 52.81% and 64.69%, respectively. The cause and explanation for this are similar to that of the pH-dependence discussed above.

When the pH of the HA electrolyte was 8.5 the galena i_{corr} decreased from 0.469 to 0.318 μA cm^{-2} and to 0.246 μA cm^{-2} with increasing HA concentration from 0 mg/L to 10 mg/L and to 100 mg/L, respectively. Finally, the corrosion density reached 0.137 μA cm^{-2} when the HA concentration was 1000 mg/L. The inhibiting efficiencies were 32.19%, 47.55% and 70.79%, respectively. When the electrolyte pH was 10.5, the galena i_{corr} decreased from 0.815 to 0.540 μA cm^{-2} and from 0.382 μA cm^{-2} to 0.243 μA cm^{-2} when the HA concentration was 1000 mg/L. The inhibiting efficiencies were 33.74%, 53.13% and 70.18%, respectively. A detailed explanation for the above phenomena is presented as follows: at the anode, the galena was oxidized according to reaction (1). Similar to that of an acidic electrolyte, a higher concentration of HA provided greater HA ionization and released more H^+ and $–COO^-$ ions. Higher concentrations of $–COO^-$ ions favor the anode reaction, which is the complexation of $–COO^-$ and Pb^{2+} ions. This complexation is why the anodic Tafel slope (b_a) decreased. At the cathode, higher concentrations of H^+ ions favor the cathode reaction (reaction (4)), causing the cathodic Tafel slope (b_c) to decrease. Corrosion potential (E_{corr}) is another important parameter to evaluate the electrochemical corrosion of a material. Generally, a more positive corrosion potential suggests that the material has better corrosion resistance. When the electrolyte pH was 2.5, as mentioned above, increasing the concentration of HA inhibited galena corrosion. As the galena corrosion current density decreased, the corrosion potential became more positive. These data suggested galena had a better corrosion resistance when increasing the concentration of HA. However, when the electrolyte pH was 4.5, 8.5 or 10.5, the galena corrosion current density decreased, and the corrosion potential changed more negatively. The corrosion potential results suggest that the corrosion

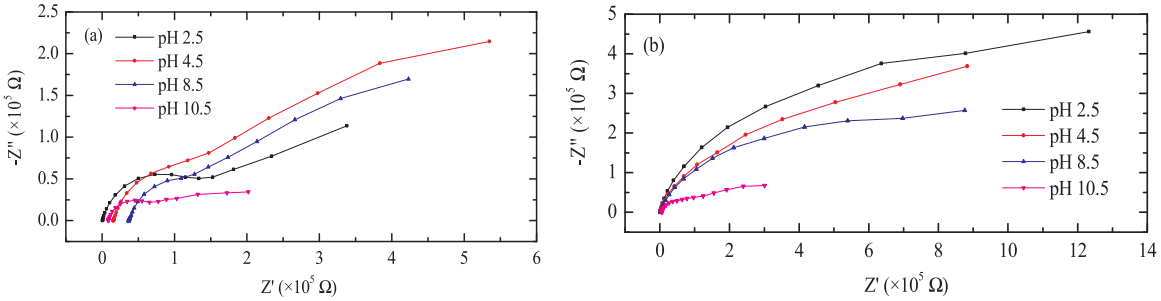

Fig. 3. Nyquist plots for galena in 0 mg/L (a) and 100 mg/L (b) HA solutions with different pH.

resistance of the galena samples decreased with increasing concentrations of HA. This is because HA has a relatively open structure and contains numerous functional groups that in aqueous solutions, especially in weakly acidic or alkaline solutions, become predominantly negatively charged (such as -COO^- ions) because of proton dissociation (Ren et al., 2015).

Fig. S1 shows the potentiodynamic curves of the galena electrode in HA solutions at different pH values. When the electrolyte contained HA, HA did not change the profiles of the potentiodynamic curves, suggesting the same electrochemical interaction mechanism. In contrast, the potentiodynamic curve shifted to the right and became more negative in the x and y directions when the pH increased, suggesting an increase in corrosion current density and a shift to more negative corrosion potential.

When the electrolyte did not contain HA (Fig. S1 (a)), the polarization parameters in Table 1 show that the galena i_{corr} increased from 0.303 to 0.398 μA cm^{-2}, as the pH decreased from 4.5 to 2.5. This indicates that higher acidity accelerates galena corrosion. The promotion efficiency was 23.87%, and the polarization resistance reduced from 167.2 to 103.0 kΩ cm^2. The causes for this phenomenon are presented as follows: (1) in acidic electrolyte, galena acted as an anode and was oxidized according to reaction (1); (2) S° was produced and absorbed on the galena electrode surface, and (3) O_2 was reduced at the cathode according to reaction (4). The higher acidity favors S° dissolution and is beneficial for the reduction of O_2. Thus, this acidity causes the anodic and cathodic Tafel slopes to decrease and ultimately results in a decrease in the polarization resistance. In alkaline electrolyte, the galena i_{corr} increased from 0.469 to 0.815 μA cm^{-2}, as pH increased from 8.5 to 10.5, and the promotion efficiency was 73.77% when the polarization resistance decreased from 168.1 to 80.7 kΩ cm^2. In contrast to the acidic electrolyte, the decrease in the polarization resistance with increasing alkalinity was because of the decrease in the anodic Tafel slope, despite the increase in the cathodic Tafel slope. A detailed explanation is as follows: in the alkaline electrolyte, O_2 was reduced via reaction (5) at the cathode. The higher concentration of OH^- ions was unfavorable for reaction (5), resulting in a larger cathodic Tafel slope. However, the higher concentrations of OH^- ions favor the galena anodic oxidation as in reactions (6) and (7), which caused the anodic Tafel slope to decrease.

$$O_2 + 2H_2O + 4e^- = 4OH^- \quad (5)$$

$$Pb^{2+} + 2OH^- = Pb(OH)_2\downarrow \quad (6)$$

$$Pb(OH)_2 + 2NaOH = Na_2[Pb(OH)_4] \quad (7)$$

When the electrolyte contained 10 mg/L, 100 mg/L and 1000 mg/L HA (Fig. S1 (b-d)), the galena polarization results in Table 1 show the galena i_{corr} increased as the HA solution pH increased. This indicates that stronger alkalinity promotes galena corrosion. Meanwhile, galena E_{corr} changed more negatively, which implies galena has excellent erosion-resistance. This erosion-resistance is because galena polarization resistance decreased as the solution pH increased.

The presence of HA had no effect on the galena electrochemical interaction mechanism. Under acidic conditions, H^+ ions at the cathode participate in O_2 reduction via reaction (4). Thus, reducing the acidity (increasing pH from 2.5 to 4.5) was unfavorable for the reduction of O_2, and this was why the cathodic Tafel slope (b_c) increased. At the anode, galena was oxidized via reaction (1), and when the pH of the HA solution increased from 2.5 to 4.5, the HA ionization changed more strongly, releasing more H^+ and –COO^- ions. This release provoked the complexation of –COO^- ions and Pb^{2+} ions, resulting in a decrease in polarization resistance. However, the increase in passivated S° inhibited the galena anodic oxidation. This, in turn, resulted in an increase in the anodic Tafel slope (b_a). Under alkaline conditions, O_2 at the cathode was reduced via reaction (5). It seemed that the cathodic Tafel slope (b_c) should increase following the pH increase from 8.5 to 10.5 for the electrolyte without HA, as higher concentrations of OH^- ions were unfavorable for reaction (5). However, due to the higher concentrations of OH^- ions, HA ionizes in the presence of the electrolyte, consuming OH^- ions and accelerating reaction (5), resulting in a decrease of the cathodic Tafel slope (b_c) At the anode, galena was oxidized via reaction (1), and when the pH of the HA solution increased from 8.5 to 10.5, the HA ionization increased, releasing more H^+ and –COO^- ions. This release provoked the complexation of –COO^- ions and Pb^{2+} ions, resulting in an anodic Tafel slope (b_a) decrease. As mentioned above, under alkaline conditions, Pb^{2+} from galena can transform into $Pb[(OH)_4]^{2-}$ via reactions (6) and (7), as well as promote anodic oxidation.

3.2. EIS study

EIS has become a ubiquitous technique for the analysis of fundamental diffusion and Faradaic reactions, such as corrosion, adsorption, and chemical reactions coupled with Faradaic processes at electrodes (Lasia, 2002). In this study, EIS studies were conducted to confirm the electrochemical corrosion processes of galena. Fig. 3(a) and Fig. 3(b) present the Nyquist plots for galena in 0 mg/L and 100 mg/L HA solutions, respectively, at different pH values. Regardless of the presence or concentration of HA, the Nyquist plots exhibited two capacitive loops. The loop at high frequency was attributed to the charge transfer resistance (R_t) corresponding to the resistance between the galena and the outer Helmholtz plane. The loop at low frequency, which is slightly distorted, is related to the combination of the pseudo-capacitance impedance (because of the passive layer) and resistance R_f. The deviation from an ideal semicircle was attributed to the frequency dispersion and the inhomogeneity of the passive layer surface. The electrochemical equivalent circuit (EEC) shown in Fig. S2 was used to model the galena/electrolyte interface. In this EEC, R_s is the ohmic resistance of the solution; R_t is the charge transfer resistance; R_f is the passive film resistance; and CPE_t and CPE_f represent the constant phase element used to replace the charge transfer capacitance at the double layer (C_t) and the passive film capacitance (C_f), respectively. The impedance of the *CPE* is given by Macdonald (1985) as:

$$Z_{CPE} = \frac{1}{Y_0(j\omega)^n} \quad (8)$$

Table 2
Equivalent circuit model parameters for galena in electrolyte without and with 100 mg/L HA.

pH	C_{HA} (mg L^{-1})	CPE_t, Y_0 (S cm^{-2} s^{-n})	n	R_t (Ω cm^2)	CPE_f, Y_0 (S cm^{-2} s^{-n})	n	R_f (Ω cm^2)
2.5	0	6.906×10^{-5}	0.8204	3.956×10^{4}	1.992×10^{-3}	1	4.647×10^{4}
	100	6.127×10^{-5}	0.8614	1.930×10^{5}	4.980×10^{-4}	1	1.078×10^{5}
4.5	0	6.463×10^{-5}	0.7950	4.998×10^{4}	4.839×10^{-4}	0.8000	1.034×10^{5}
	100	6.316×10^{-5}	0.8000	1.848×10^{5}	4.247×10^{-4}	0.8000	1.200×10^{5}
8.5	0	6.069×10^{-5}	0.7857	3.550×10^{4}	4.537×10^{-4}	0.7986	6.067×10^{4}
	100	5.776×10^{-5}	0.8155	9.142×10^{4}	5.519×10^{-6}	0.9023	6.419×10^{4}
10.5	0	8.465×10^{-5}	0.8000	2.018×10^{4}	1.680×10^{-3}	0.8012	2.320×10^{4}
	100	6.537×10^{-5}	0.8221	6.685×10^{4}	9.575×10^{-4}	0.8000	4.568×10^{4}

Here, Z_{CPE} is the impedance of the constant phase element (Ω cm^2); ω is the angular frequency of the AC voltage (rad s^{-1}); Y_0 is the magnitude of admittance of the *CPE* (Ω^{-1} cm^{-2} S^{-n}); and n is a dimensionless number, the *CPE* is considered ideal capacitance when $n = 1$. Pang et al. (1990) provides a detailed theoretical explanation for this EEC, and Constantin and Chirita (2013) even used it to model the electrochemical corrosion of pyrite in acidic media. The impedance parameters obtained by fitting the EIS data to the equivalent circuit are listed in Table 2.

Comparing the galena electrochemical parameters in 0 mg/L and 100 mg/L HA solutions, we can see that whether the electrolyte was acidic (pH 2.5 or 4.5) or alkaline (pH 8.5 or 10.5), increasing the concentration of HA led to an increase in the R_t value and a decrease in the double-layer capacitance (CPE_t, Y_0). The increase in the R_t value indicates that ions change after transport through the double-charge layer. The decrease in CPE_t, Y_0 was attributed to the decrease in the local dielectric constant of the electrical double layer. The lower capacitance and the greater resistance of the double layer indicate that increasing the concentration of HA weakened the galena electrochemical oxidation. Furthermore, increasing the concentration of HA caused greater passive film resistance (R_f) and smaller passive capacitance (CPE_f, Y_0). The smaller capacitance and the greater resistance of the film on the electrode surface indicate a more dense passive film. All of these results agree with the polarization results.

When the electrolyte did not contain HA in the double-charge layer, increased electrolyte acidity (pH decrease from 4.5 to 2.5) or alkalinity (pH increase from 8.5 to 10.5) resulted in smaller charge transfer resistance (R_t) and greater double-layer capacitance (CPE_t, Y_0). This result indicates that ions can be easily transported through the double-charge layer. Furthermore, in the passive film, increased electrolyte acidity or alkalinity also caused smaller passive resistance (R_f) and greater passive film capacitance (CPE_f, Y_0), suggesting a looser passive film. All of these results agree with the polarization results that higher acidity/alkalinity accelerates galena electrochemical corrosion.

When the electrolyte contained 100 mg/L HA in the double-charge layer, in contrast to the electrolyte without HA, the decreased electrolyte acidity (pH increase from 2.5 to 4.5) or increased alkalinity (pH increase from 8.5 to 10.5) resulted in smaller charge transfer resistance R_t and larger double-layer capacitance (CPE_t, Y_0). These results indicate that ions can be easily transported through the double-charge layer to the passive film, leading to smaller passive resistance R_f and larger passive film capacitance (CPE_f, Y_0), suggesting a looser passive film. The results reveal that stronger alkalinity increases galena corrosion when the electrolyte contains HA, which is consistent with the results of the solution analysis.

3.3. Surface characterization measurements

In order to analyze the interaction between Pb (II) and HA particles, FTIR spectra of HA-Pb (II) were obtained and compared with the FTIR spectrum of HA. Fig. 4 shows the FTIR spectra of the massive galena electrodes after weathering in pH 4.5 and pH 8.5 solutions with different concentrations of HA. When no HA was present, the FTIR spectroscopic proved the black solutions no HA group band. It is worth noting that the bands between 2000 cm^{-1} and 2500 cm^{-1} are attributed to CO_2, as the test was performed in air. To HA, the FTIR spectroscopic data exhibited three distinct peaks, namely, carboxyl at 1600 cm^{-1} (–COO^- stretch and possibly aromatic C=C stretch), phenol at 1385 cm^{-1} and 1035 cm^{-1}, and saturated group (–CH_2 symmetric stretching and asymmetric stretching region 2840–2940 cm^{-1}) (Baes and Bloom, 1989; Niemeyer et al., 1992).

At pH 4.5 and in the presence of HA, the galena sample weathered for 10 weeks exhibited three pronounced spectral features: (1) a new vibration peak at 1710 cm^{-1}, which was attributed to –C=O stretch in COOH (Swift, 1996), the cause was –COO^- and H^+ band to –COOH group; (2) compare with another appeared simultaneously wavenumber band 1385 cm^{-1}, the peak at 1035 cm^{-1} almost disappeared for HA and Pb (II) ions complex; (3) the peak at 1600 cm^{-1} for HA carboxyl group shifted to a unresolved band at about 1458 cm^{-1}, which further confirmed the formation of HA-Pb(II) complexes. The Δ parameter value was 142 cm^{-1}, indicating the formation of bridging complexes (Fig. 1a) (Nakamoto, 1989). Jerzykiewicz (2004) obtained a similar result in the study of HA interactions with Pb (II) ions.

At pH 8.5 and in the presence of HA, the galena sample weathered for 10 weeks exhibited the following spectral features: (1) when no additional Pb^{2+} ions were added, whether in 10 mg/L or in 100 mg/L HA soak solution, no HA or HA-Pb (II) occur. This is because Pb^{2+} ions from PbS were oxidized and transformed into $Pb(OH)_2$, which further proved the oxidation process of galena and produce more S°. S^0 film covered on galena surface and thus resisted HA adsorbed on galena surface; (2) when 1 mg/L Pb^{2+} ions were added to the HA solution, on one hand, the added Pb^{2+} ions inhibit galena oxidation, not enough S film covered the galena surface. On the other hand, the added Pb^{2+} ions can interaction with HA, and causing a similar FTIR result as that in pH 4.5.

Fig. 5 shows the Raman spectra of pristine and weathered galena samples. In the pristine samples, Raman active phonon for the cubic structure of galena was not observed. After the samples were weathered for 10 weeks, the galena sample weathered at pH 4.5 with 100 mg/L HA exhibited three Raman peaks at 152 cm^{-1}, 216 cm^{-1} and 437 cm^{-1} (Fig. 5(a)). The Raman peaks at 152 cm^{-1} and 216 cm^{-1} were assigned to the vibration mode of the S-S bond of elemental sulfur (Li et al., 1993). The Raman peak at 437 cm^{-1} is characteristic of a structure for the anglesite species (Shapter et al., 2000; Batonneau et al., 2000). At pH 4.5 and without HA, the galena spectrum exhibited broad Raman peaks at 435–447 cm^{-1}, 610 cm^{-1}, 975 cm^{-1} and 1051 cm^{-1} (Fig. 5(b)). All peaks were assigned to the anglesite species (Shapter et al., 2000; Batonneau et al., 2000). Comparing the galena spectra in acidic conditions with and without HA, galena is oxidized to sulfur during the initial step and ultimately transformed into anglesiteuring the galena weathering process. HA can easily adsorb on the galena surface and inhibit its transformation into sulfur, as well as inhibit galena weathering. These results are in good agreement with the above electrochemical results. When the solution pH was 8.5 and contained 100 mg/L HA, the galena Raman spectrum exhibited two typical Raman peaks of anglesite at 435–439 cm^{-1} and 973 cm^{-1} (Fig. 5(c)).

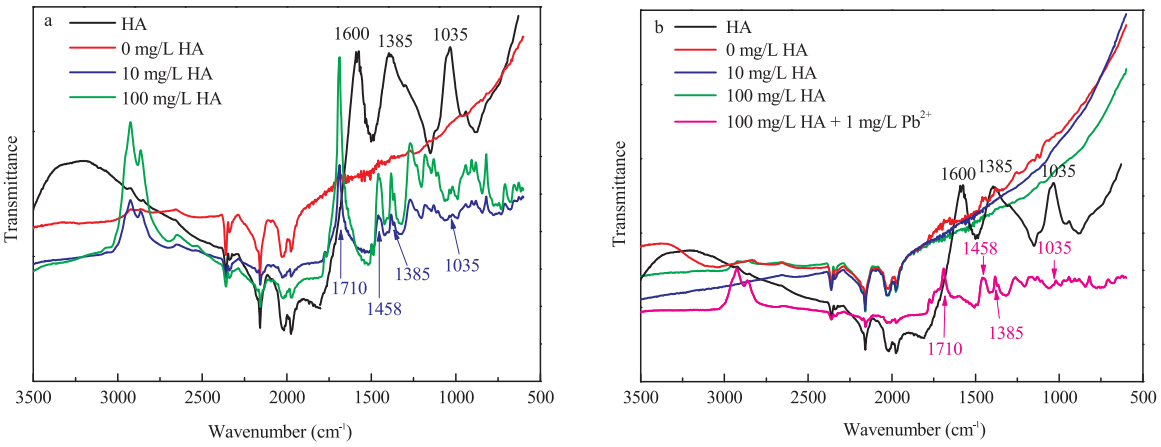

Fig. 4. FTIR spectra of galena after weathering 10-weeks in (a) pH 4.5 and (b) pH 8.5 solutions with different concentrations of HA.

However, when the solution did not contain HA, three different peaks were observed (Fig. 5(d)). The peak at 216 cm^{-1} was assigned to sulfur as mentioned above, and the peak at 291 cm^{-1} resulted from the orthorhombic β-PbO species. The third peak at 346 cm^{-1} resulted from tetragonal α-PbO species (Wiechert et al., 2005). The galena spectra under alkaline conditions with and without HA revealed two different weathering mechanisms. At the initial step, galena is oxidized to sulfur and Pb^{2+}. When the solution contained HA, sulfur can be further reduced to sulphate ions because of the HA ionization effect. Then, SO_4^{2-} and Pb^{2+} combine to form $PbSO_4$. However, in the solution without HA, sulfur cannot be reduced, and Pb^{2+} combines with OH^- to form $Pb(OH)_2$. During the Raman spectroscopic measurements, it seemed that $Pb(OH)_2$ might be in the form of $PbO{\cdot}H_2O$, and its Raman peak manifests as a waveform of PbO. All of these results are consistent with the electrochemical results. As stated above, Fig. S3 shows galena the weathering mechanism with and without HA via electrochemical and surface analyses.

3.4. Environmental risk assessment based on in situ electrochemical and surface investigation

In nature, galena and HA usually occur together. Galena weathering releases Pb^{2+} and causing heavy metal ions pollution. HA can bind metal ions; therefore, the environmental issues from galena (include

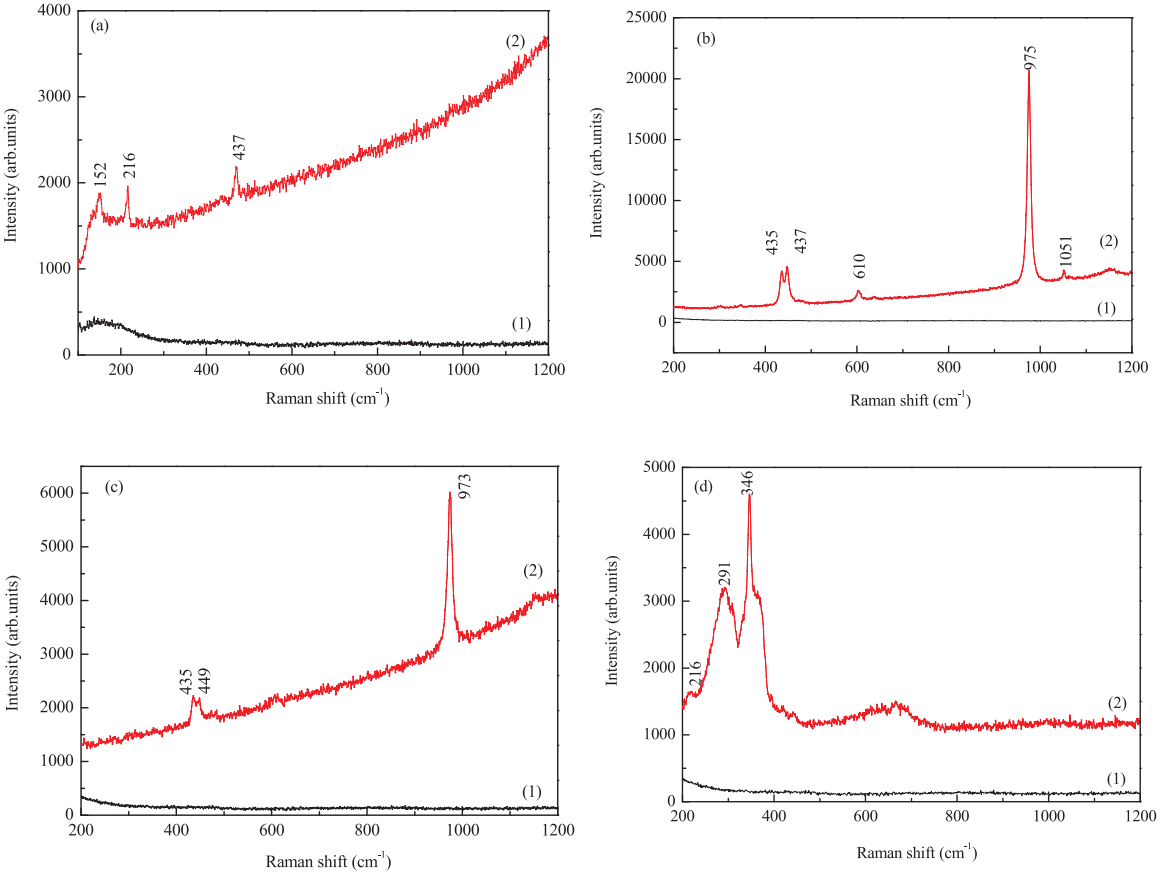

Fig. 5. Raman spectra of the massive galena electrodes after weathering in different acid/alkaline solutions with/without HA. Where: (a) pH 4.5 with 100 mg/L HA, (b) pH 4.5 without HA, (c) pH 8.5 with 100 mg/L HA and (d) pH 8.5 without HA for: (1) pristine surface; (2) 10-weeks leached surfaces.

other metal sulfide minerals) weathering must be affected by the presence of HA. At present, acid mine drainage is one of the serious environmental issues surrounding metal sulfide mineral mining, and the accumulated H^+ ions will accelerate galena weathering and aggravate heavy metal ion pollution. The presence of HA can inhibit galena weathering and, thus, mitigate environmental pollution in mining districts and the surrounding areas.

Generally speaking, higher acidity or higher alkalinity promotes galena corrosion and results in more serious environmental issues during galena weathering process. In the future, HA, especially after physical-chemical modification may be a good adsorbent for toxic heavy metals. Depending on the corrosion current density i_{corr}, the galena weathering rate could be calculated according to the Faraday equation (Eq. 9) (Gunawarman et al., 2016):

$$v = \frac{Mi_{corr}}{nF} \quad (9)$$

where v is the weathering rate in $g\,m^{-2}\,h^{-1}$, i_{corr} is corrosion current density in $\mu A\,cm^{-2}$, M is the atomic weight in g·mol, n is the valence state, and F is the Faraday constant (96,487 C mol). For example (Table 1), for a solution pH of 2.5 without HA, galena i_{corr} was $0.398\ \mu A\,cm^{-2}$. Thus, the galena weathering rate was $0.015\ g\,m^{-2}\,h^{-1}$. Therefore, when the galena area is $1\ m^2$, it will release 134.7 g Pb^{2+} to the surrounding environment per year. When the solution contained 1000 mg/L HA, galena i_{corr} decreased to $0.083\ \mu A\,cm^{-2}$, and the galena weathering rate was $0.0032\ g\,m^{-2}\,h^{-1}$. Based on the calculations, the amount of Pb^{2+} released will decrease to 28.09 g per year, under the same conditions. This method could be used to assess how much Pb^{2+} ions will be released over a certain time and how much HA is required to mitigate the release of Pb^{2+}. In addition, this method can be applied to soil, if the content of galena in the soil is known.

4. Conclusions

Galena weathering was studied under acidic and alkaline conditions depending on electrochemical method combined with spectroscopic techniques, with and without HA. The polarization curve and EIS revealed that HA inhibits galena weathering for causing greater polarization resistance and passive film resistance. HA doesn't change galena weathering mechanism under acidic conditions, and changes the galena weathering mechanism via ionization effect under alkali conditions. Galena weathering releases 134.7 $g/m^2/y$ Pb^{2+} to the surrounding environment when pH is 2.5, and the amount released decreases to 28.09 g in the presence of 1000 mg/L HA. The FTIR spectra and Raman spectra revealed that HA and Pb (II) ions form bridging complexes under acidic conditions. Under alkali conditions without HA, galena weathering ultimate products are S^0 and $PbO{\cdot}H_2O$, and the ultimate product is anglesite the presence of HA.

Acknowledgment

This work was financially supported by the National Key R&D Program of China (Grant No. 2016YFC0600104, Large-scale Scientific Apparatus Development Program of Chinese Academy of Sciences (Grant No. YZ200720), and the "135" Program of the Institute of Geochemistry, Chinese Academy of Sciences (CAS). We would like to thank LetPub (www.letpub.com) for providing linguistic assistance during the preparation of this manuscript.

Appendix A. Supplementary material

Supplementary data associated with this article can be found in the online version at http://dx.doi.org/10.1016/j.ecoenv.2018.04.030.

References

Acai, P., Sorrenti, E., Gorner, T., Polakovica, M., Kongolo, M., Donato, P.D., 2009. Pyrite passivation by humic acid investigated by inverse liquid chromatography. Colloids Surf. A: Physicochem. Eng. 337, 39–46.
Acero, P., Cama, J., Ayora, C., 2007. Rate law for galena dissolution in acidic environment. Chem. Geol. 245, 219–229.
Apak, R., 2002. Encyclopedia of Surface & Colloid Science (invited review). Dekker, New York, pp. 385.
Azhari, A.E., Rhoujjati, A., Hachimi, M.L.E., Ambrosi, J.P., 2017. Pollution and ecological risk assessment of heavy metals in the soil-plant system and the sediment-water column around a former Pb/Zn-mining area in NE Morocco. Ecotoxicol. Environ. Saf. 144, 464–474.
Baes, A.U., Bloom, P.R., 1989. Diffuse reflectance and transmission fourier transform infrared (DRIFT) spectroscopy of humic and fulvic acids. Soil Sci. Soc. Am. J. 53, 695–700.
Bard, A.J., Faulkner, L.R., 2001. Electrochemical Methods: Fundamentals And Applications, 2nd. Wiley and Sons, Hoboken.
Batonneau, Y., Brémard, C., Laureyns, J., Merlin, J.C., 2000. Microscopic and imaging Raman scattering study of PbS and its photo-oxidation products. J. Raman Spectrosc. 31, 1113–1119.
Benvenuti, M., Mascaro, I., Corsini, F., Ferrari, M., Lattanzi, P., Parrini, P., Costagliola, P., Tanelli, G., 2000. Environmental mineralogy and geochemistry of waste dumps at the Pb(Zn)-Ag Bottino mine, Apuane Alps, Italy. Eur. J. Miner. 12, 441–453.
Bergeron, M., Harrison, Y., 1989. Le transport chimique de l'or dans les environments de surface: formation d'un colloïde et complexation organique. Can. J. Earth Sci. 26, 2327–2332.
Celebi, O., Erten, H.N., 2010. Sorption of phenol and radioactive cesium onto surfactant modified insolubilized Modifying hydroxyapatite nanoparticles with humic acid. J. Radioanal. Nucl. Chem. 284, 669–675.
Chotpantarat, S., Chunhacherdchai, L., Rakkreat Wikiniyadhanee, R., Tongcumpou C., 2015. Effects of humic acid amendment on the mobility of heavy metals (Co, Cu, Cr, Mn, Ni, Pb, and Zn) in gold mine tailings in Thailand. 8, 7589-7600.
Constantin, C.A., Chirita, P., 2013. Oxidative dissolution of pyrite in acidic media. J. Appl. Electrochem. 43, 659–666.
Fornasiero, D., Li, F., Ralston, J., Smart, R.S.C., 1994. Oxidation of galena surfaces: I. X-ray photoelectron spectroscopic and dissolution kinetics studies. J. Colloid Interface Sci. 164, 333–344.
Genc-Fuhrman, H., Mikkelsen, P.S., Ledin, A., 2016. Simultaneous removal of As, Cd, Cr, Cu, Ni and Zn from stormwater using high-efficiency industrial sorbents: effect of pH, contact time and humic acid. Sci. Total. Environ. 566, 76–85.
Gerson, A.R., O'Dea, A.R., 2003. A quantum chemical investigation of the oxidation and dissolution mechanisms of galena. Geochim. Cosmochim. Acta 67, 813–822.
Gunawarman, G., Refieska, A., Ilhamdi, I., Affi, J., Cho, K., Nakai, M., Hermawan, H., Niinomi, M., 2016. Corrosion behavior of new beta type Ti-29Nb-13Ta-4.6Zr alloy in simulated body fluid solution. Conference: Frontiers in Bioengineering and Biotechnology, January.
Heidel, C., Tichomirowa, M., 2011. Galena oxidation investigations on oxygen and sulphur isotopes. Isot. Environ. Health Stud. 47, 169–188.
Hizal, J., Apak, R., 2006. Modeling of copper (II) and lead (II) adsorption on kaolinite-based clay minerals individually and in the presence of humic acid. J. Colloid Interface Sci. 295, 1–13.
Hsieh, Y.H., Huang, C.P., 1989. The dissolution of PbS (s) in dilute aqueous solutions. J. Colloid Interface Sci. 131, 537–549.
Huang, S., Song, S., Zhang, R., Wen, T., Wang, X., Yu, S., Song, W., Hayat, T., Alsaedi, A., Wang, X., 2017. Construction of layered double hydroxides/hollow carbon microsphere composites and its applications for mutual removal of Pb (II) and humic acid from aqueous solutions. ACS Sustain. Chem. Eng. 5, 11268–11279.
Jerzykiewicz, M., 2004. Formation of new radicals in humic acids upon interaction Pb (II) ions. Geoderma 122, 305–309.
Jiang, W.J., Cai, Q., Xu, W., Yang, M.W., Cai, Y., Dionysiou, D.D., Kevin, E.O., 2014. Cr (VI) adsorption and reduction by humic acid coated on magnetite. Environ. Sci. Technol. 48, 8078–8085.
Keim, M.F., Markl, G., 2015. Weathering of galena: mineralogical processes, hydrogeochemical fluid path modeling, and estimation of the growth rate of pyromorphite. Am. Miner. 100, 1584–1594.
Koopal, L., Saito, T., Pinheiro, J., Riemsdijk, W.V., 2005. Ion binding to natural organic matter: general considerations and the NICA-Donnan model. Colloids Surf. Acta 265, 40–54.
Lara, R.H., Briones, R., Monroy, M.G., Mullet, M., Humbert, B., Dossot, M., Naja, G.M., Cruz, R., 2011. Galena weathering under simulated calcareous conditions. Sci. Total Environ. 409, 3971–3979.
Lasia, A., 2002. Electrochemical impedance spectroscopy and its applications. Mod. Asp. Electrochem. 32, 143–248.
Lei, Y., Wei, Z.G., Zhong, W.H., Cui, J., Wei, W., 2016. Modifying hydroxyapatite nanoparticles with humic acid for highly efficient removal of Cu (II) from aqueous solution. Colloids Surf. A Physicochem. Eng. Asp. 490, 9–21.
Li, J., Zhu, X., Wadsworth, M.E., 1993. Raman spectroscopy of natural and oxidized metal sulfides. In: J.P., Hager (Ed.), EPD Congress, the Minerals, Metals and Materials Society. PP, 229-244.
Li, Y.J., Yang, C., Guo, X.T., Dang, Z., Li, X.Q., Zhang, Q., 2015. Effects of humic acids on the aggregation and sorption of nano-TiO_2. Chemosphere 119, 171–176.
Liu, A., Gonzalez, R.D., 2000. Modeling adsorption of copper (II), cadmium (II) and lead (II) on purified humic acid. Langmuir 16, 3902–3909.
Liu, Q.Y., Jin, G.H., Zheng, K., Wen, X.Y., Li, H.P., 2017. Influence of temperature and

added potential on the electrochemical dissolution of galena in HNO_3 at pH 2.0 and its applied implications. Int. J. Electrochem. Sci. 12, 7004–7016.
Macdonald, J.R., 1985. Generalizations of "universal dielectric response" and a general distribution-of-activation-energies model for dielectric and conducting systems. J. Appl. Phys. 58, 1971–1978.
Martin, D.P., Seiter, J.M., Lafferty, B.J., AJ Bednar, A.J., 2017. Exploring the ability of cations to facilitate binding between inorganic oxyanions and humic acid. Chemosphere 166, 192–196.
Mikhlin, Y.L., Romanchenko, A.S., Shagaev, A.A., 2006. Scanning probe microscopy studies of PbS surfaces oxidized in air and etched in aqueous acid solutions. Appl. Surf. Sci. 252, 5645–5658.
Muñoz, J.A., Go´mez, C., Ballester, A., Bla´zquez, M.L., Gonza´lez, F., Figueroa, M., 1998. Electrochemical behaviour of chalcopyrite in the presence of silver and Sulfolobus bacteria. J. Appl. Electrochem. 28, 49–56.
Nakamoto, K., 1989. Infrared and Raman Spectra of Inorganic and Coordination Compounds. Wiley, New York, pp. 231.
Niemeyer, J., Chen, Y., Bollag, J.M., 1992. Characterization of humic acids composts and peat by diffuse reflectance fourier-transform infrared spectroscopy. Soil Sci. Soc. Am. J. 56, 135–140.
Ondrasek, G., Rengel, Z., Romi, D., 2018. Humic acids decrease uptake and distribution of trace metals, but not the growth of radish exposed to cadmium toxicity. Ecotoxicol. Environ. Saf. 151, 55–61.
Pandey, A.K., Pandey, S.D., Misra, V., 2000. Stability constants of metal humic acid complexes and its role in environmental detoxification. Ecotoxicol. Environ. Saf. 47, 195–200.
Pang, J., Briceno, A., Chander, S., 1990. A study of pyrite solution interface by impedance spectroscopy. J. Electrochem. Soc. 137, 3447–3455.
Paul, R.L., Nicol, M.J., Diggle, J.W., Saunders, A.P., 1978. The electrochemical behaviour of galena (lead sulphide) - I. Anodic dissolution. Electrochim. Acta 23, 625–633.
Ren, Z.L., Tella, M., Bravin, M.N., Comans, R.N., Dai, J., Garnier, J.M., Sivry, Y., Doelsch, E., Straathof, A., Benedetti, M.F., 2015. Effect of dissolved organic matter composition on metal speciation in soil solutions. Chem. Geol. 398, 61–69.
Ryan, J.A., Zhang, P., Hesterberg, D., Chou, J., Sayers, D.E., 2001. Formation of chloropyromorphite in a lead-contaminated soil amended with hydroxyapatite. Environ. Sci. Technol. 35, 3798–3803.
Sahoo, P.K., Kim, K., Equeenuddin, S.M., Michael, A.P., 2013. Current approaches for mitigating acid mine drainage. Rev. Environ. Contam. Toxicol. 226, 1–32.
Schulten, H.R., Schnitzer, M., 1997. Chemical model structures for soil organic matter and soils. Soil Sci. 162, 115–130.
Shapter, J.G., Brooker, M.H., Skinner, W.M., 2000. Observation of the oxidation of galena using Raman spectroscopy. Int. Miner. Process. 60, 199–211.
Solmaz, R., Kardaş, G., Yazici, B., Erbil, M., 2008. Adsorption and corrosion inhibitive properties of 2-amino-5-mercapto-1, 3, 4-thiadiazole on mild steel in hydrochloric acid media. Colloids Surf. A: Physicochem. Eng. 312, 7–17.
Stern, M., Geary, A.L., 1957. Electrochemical polarization. 1. A theoretical analysis of the shape of polarization curves. J. Electrochem. Soc. 104, 56–63.
Sutton, R., Sposito, G., 2005. Molecular structure of soil humic substances: the new view. Environ. Sci. Technol. 39, 9009–9015.
Swift, R.S., 1996. Organic matter characterization. In: In: Sparks, D.L. (Ed.), Methods of soil analysis. Part 3. Chemical Methods. SSSA Book Series no. 5 5. SSSA and ASA, Madison, WI, pp. 1011–1069.
Szczerba, M., Sawlowicz, Z., 2009. Remarks on the origin of cerussite in the upper silesian Zn-Pb deposits, Poland. Mineralogia 40, 54–64.
Tipping, E., Rey-Castro, C., Bryan, S.E., Hamilton-Taylor, J., 2002. Al(III) and Fe(III) binding by humic substances in freshwaters, and implications for trace metal speciation. Geochim. Cosmochim. Acta 66, 3211–3224.
Wang, L.Y., Liu, Q.Y., Zheng, K., Li, H.P., 2016. Assessing the influence of calcium fluoride on pyrite electrochemical dissolution and mine drainage pH. J. Environ. Qual. 45, 1344–1350.
Wiechert, D.F., Grabowski, S.P., Simon, M., 2005. Raman spectroscopic investigation of evaporated PbO layers. Thin Solid Films 484, 73–82.
Yang, R., Van Den Berg, C.M.G., 2009. Metal complexation by humic substances in seawater. Environ. Sci. Technol. 43, 7192–7197.